ASME Journal of Dynamic Systems, Measurement, and Control
Online journal at:
https://asmedigitalcollection.asme.org/dynamicsystems

Wanqun Yang
Electrical and Computer Engineering,
Oakland University,
Rochester, MI 48309
e-mail: wanqunyang@oakland.edu

Ranya Badawi
Electrical and Computer Engineering,
Oakland University,
Rochester, MI 48309
e-mail: ranyabadawi@oakland.edu

Jun Chen[1]
Electrical and Computer Engineering,
Oakland University,
Rochester, MI 48309
e-mail: junchen@oakland.edu

Event-Triggered Model Predictive Control of a Buck Converter With Kalman Filter State Estimation

This paper presents an event-triggered model predictive control (ET-MPC) strategy for a DC–DC buck converter to reduce computational burden while maintaining high dynamic performance. A four-mode discrete-time model is established to accurately capture the converter switching behavior, and a Kalman filter is integrated into the control framework to estimate load disturbances and improve control accuracy. Unlike conventional time-triggered MPC (TT-MPC), which solves an optimization problem at every time-step, the proposed ET-MPC evaluates the optimal switching sequence only when a voltage deviation exceeds a predefined threshold. This mechanism significantly reduces the number of online optimizations while preserving the regulation of output voltage. Simulation results demonstrate that ET-MPC achieves up to 94% reduction in computational effort with comparable transient response, low steady-state error, and acceptable switching frequency. The proposed controller enables an efficient real-time implementation of model predictive control (MPC) for power converters under varying operating conditions.
[DOI: 10.1115/1.4071872]

1 Introduction

Power converters are widely used in electric vehicles, renewable energy systems, and energy storage applications because they can efficiently control the flow of electrical power [1]. The performance of a converter mainly depends on its control strategy, which determines how fast the system can respond to changes, how accurately the output voltage or current is regulated, and how stable the system remains under disturbances [2–4]. A good control method can improve power efficiency, reduce losses, and ensure reliable operation over a wide range of operating conditions [3]. Therefore, developing effective control strategies for power converters is essential for achieving high performance, high reliability, and low-cost power conversion systems [5].

However, traditional control methods such as proportional–integral (PI), hysteresis, and droop control are designed for a specific operating condition, and they assume the system has ideal behavior [6–10]. These methods have a limited ability to deal with nonlinear characteristics, parameter variations, and control constraints, which may result in poor dynamic response and reduced steady-state accuracy in practical applications. For example, Aguilar-Ibanez et al. [6] investigate PI-based control strategies for DC–DC converters and introduce improved modulation techniques to enhance voltage regulation. However, the method is still developed based on averaged linear modeling and fixed gain tuning, which limits its ability to handle nonlinear dynamics. Because of these limitations, advanced control methods are needed to maintain good performance even when operating conditions change.

Model predictive control (MPC) is an advanced control strategy for power converters that has received significant attention in recent years [11–13]. MPC is a flexible approach that utilizes a mathematical model of the converter and a control objective to compute the optimal control action. This is achieved by minimizing a cost function that evaluates the system behavior over a finite prediction horizon [14]. In traditional MPC, the optimization problem is solved at each sampling period, and only the first control signal in the optimal control sequence is applied to the converter. The predictive nature of the controller enables fast transient response and accurate steady-state regulation [15]. Moreover, MPC can effectively control systems with multiple inputs and multiple outputs by capturing the interactions among variables through the system model.

Nevertheless, traditional MPC still suffers from a high computational burden in the converter field since a large number of switching possibilities must be evaluated within each sampling period, which is typically in the microsecond range [16,17]. This leads to a heavy computational burden, especially when the converter operates at a high switching frequency and the sampling period is only a few microseconds [17]. The problem becomes more significant for converters with nonminimum phase behavior such as boost and buck–boost converters [17–19]. In these converters, turning the main switch ON causes a short voltage drop before recovery after several switching cycles, resulting in a slower transient response. This delay increases the prediction complexity and often requires extending the switching-sequence prediction horizon. As the horizon increases, the number of switching combinations also grows rapidly, which further raises the computational cost. As a result, traditional MPC is difficult to apply in practical converter systems.

To lower the computational burden of conventional time-triggered MPC (or TT-MPC), event-triggered MPC (or ET-MPC) has been introduced to reduce computational load by updating the control action only when a predefined condition is violated, rather than at every sampling period. This strategy has been widely studied and applied across different control systems [13,20–28]. In these

[1]Corresponding author.
Manuscript received October 27, 2025; final manuscript received April 24, 2026; published online July 24, 2026. Assoc. Editor: Afef Fekih.

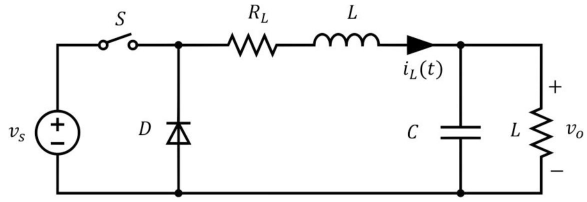

Fig. 1 Buck converter circuit diagram

works, the event-trigger mechanism significantly decreases the number of optimization problems solved while preserving control accuracy. For example, Badawi and Chen [29–31] implement ET-MPC on a boost converter and report that it can achieve similar control performance compared to the conventional TT-MPC. They also observe a significant reduction in computational effort. In Ref. [20], an event-triggered control strategy is embedded into the predictive controller for a modular multilevel converter. When the power tracking error (T.E.) stays within a predefined threshold, the previous control input is retained; a new MPC optimization is executed only when the threshold is violated. This event-based strategy effectively reduces switching frequency and energy loss while maintaining accurate regulation under parameter variations.

Furthermore, MPC critically depends on an accurate dynamic model of the system to predict optimal control actions. These optimal actions are determined by the accurate initial state sent to the system [15]. The initial state may be obtained either through direct measurements or via a state observer for variables that cannot be directly measured [32]. However, both approaches can be affected by measurement noises, sensor inaccuracies, and component tolerances, leading to errors in the estimated system states [33]. Therefore, state estimation plays an essential role in MPC by using past measurements and system dynamics to infer the most probable current state, thus improving control reliability. State estimators are generally categorized into deterministic estimators (such as the Luenberger filter) and stochastic estimators (such as the Kalman filter) [34,35]. Among these methods, the Kalman filter has been widely recognized as an effective estimator in systems subject to high model uncertainty and significant noise [36,37]. In our work, we integrate the Kalman filter into our ET-MPC control framework.

The target of this study is to design an ET-MPC controller for a buck converter. A buck converter is a step-down converter that provides an output voltage that is less than its input voltage [38]. It is prevalent in power conversion applications since power is transmitted more efficiently at higher voltages while loads typically require lower voltages for operation, either for safety or other reasons [39]. Buck converters can be found in many applications such as battery chargers, computers, and audio amplifiers [40–42]. Isolated buck-derived converters, such as full-bridge isolated converters, are found in hybrid and electric vehicles, and can convert power from the 400 V battery to charge the 12 V battery and provide power to the 12 V bus. The topology of a DC–DC buck converter is shown in Fig. 1. It consists of a DC voltage source v_s, a switch S, a diode D, an inductor L with internal resistance R_L, a capacitor C and a load resistor R. We also benchmark the ET-MPC controller with an enumeration-based TT-MPC controller, as illustrated in Fig. 2. It operates using a discrete-time model of the converter. At each sampling period, the controller generates a finite set of switching sequences over the prediction horizon, defined as $N \cdot T_s$, where N is the number of switching intervals and T_s is the sampling period. For each switching sequence, the model predicts the future evolution of the inductor current and output voltage over the prediction horizon. These predicted trajectories are then evaluated through an optimal control problem, which selects the switching sequence that provides the best voltage regulation while satisfying system objectives and operational constraints.

In the sequel, we will first develop the main components of the TT-MPC controller for the buck converter, followed by the development of the proposed ET-MPC controller. The proposed approach follows the same design but adapts the framework to the buck converter topology, which operates with continuous and discontinuous conduction modes. A concise comparison table including the triggering condition, modeling approach, use of disturbance estimation (e.g., recursive least squares, extended state observer, or reduced-order extended state observer), and computational metrics is provided as Table 1 to strengthen the contribution. The main contributions of this paper can be summarized as follows:

(1) A four-mode switched discrete-time model of the buck converter is developed and embedded into the MPC framework. The proposed model explicitly captures both continuous conduction mode and discontinuous conduction mode, rather than relying on an averaged model commonly adopted in existing ET-MPC studies [13,45].
(2) A trajectory-based event-triggered MPC framework is proposed for enumeration-based MPC with move blocking. The triggering condition is defined based on the deviation between the measured output voltage and the previously computed optimal predicted trajectory.

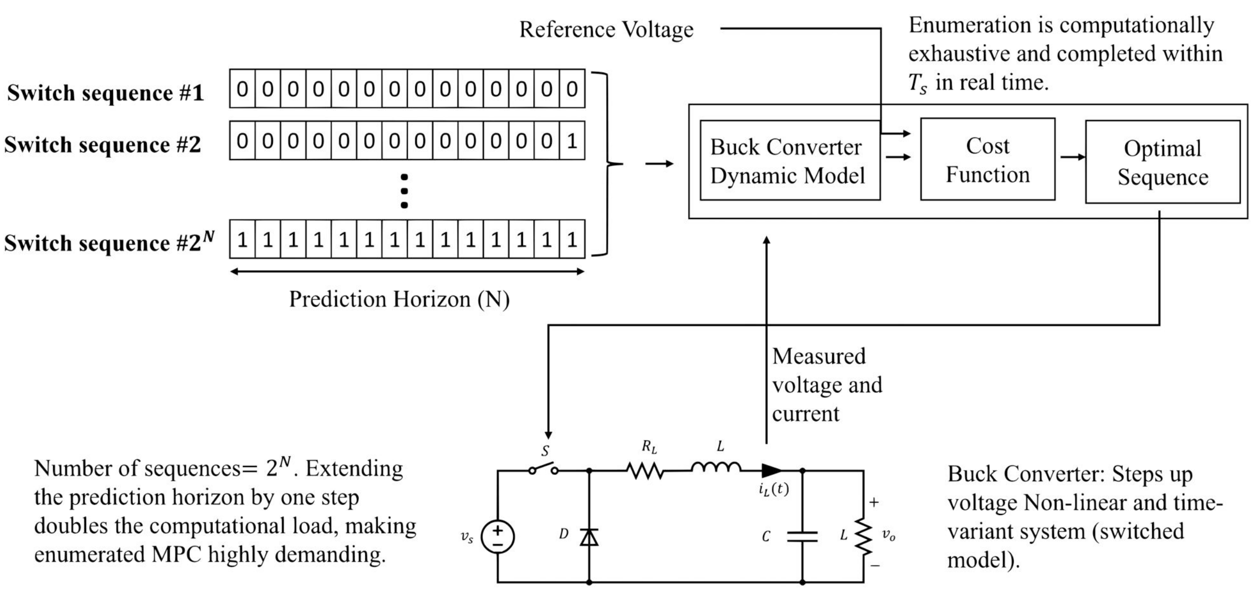

Fig. 2 Enumeration-based model predictive control for a buck converter

Table 1 Comparison of ET-MPC frameworks for power converters

Feature	Ref. [43]	Ref. [13]	Ref. [44]	Ref. [45]	Our work
Triggering condition	State-error threshold	State-error threshold	State-error threshold	Disturbance-aware error bound	Predicted-trajectory deviation
Modeling approach	Switched model	Averaged model	Switched model	Averaged model	Switched model; CCM/DCM
Disturbance estimation	None	None	RLS	ESO/RESO	Kalman filter
Computational metrics	Event count; switching reduction	Event count; switching actions	Event count	Event count	Event rate; min interevent interval

(3) A Kalman filter state estimator is incorporated into the proposed control framework to improve robustness against load variations and measurement noise.
(4) The effectiveness of the proposed approach is validated through simulations, demonstrating a substantial reduction in online optimization calls while maintaining comparable transient and steady-state performance to time-triggered MPC (TT-MPC). The proposed approach reduces the computational burden by up to 94% compared with the conventional TT-MPC.

The remainder of this paper is organized as follows: Section 2 presents the mathematical modeling of the buck converter and the derivation of its discrete-time system dynamics. Section 3 describes the formulation of the proposed model predictive control schemes, including both time-triggered and event-triggered implementations. Section 4 provides the simulation setup, implementation details, and performance evaluation under different operating conditions. Finally, Sec. 5 concludes the paper and discusses potential directions for future work.

2 Mathematical Model

2.1 Continuous-Time Model. For MPC to generate optimal control actions at every sampling period T_s, a reliable mathematical representation of the system plant is required. Since switched-mode power converters exhibit nonlinear and time-varying characteristics, their modeling typically involves simplifying the switching behavior while keeping the essential system dynamics. A widely adopted approach in the control of pulse-width modulation (PWM) converters is to create an AC equivalent circuit by averaging the inductor voltage and capacitor current over one switching cycle [46].

For the buck converter shown in Fig. 1, three operating modes can be identified within each switching period depending on the state of the main switch S and the inductor current during a single time step T_s. The first mode is when the switch is ON and the inductor current is positive and increasing. In this mode, the diode is OFF. The second mode is when the switch is OFF. In this case, the inductor will induce a voltage that will force the current to continue flowing in the same direction through the diode to the load. The third mode is when the switch is OFF, and the inductor current reaches zero; in this case, the diode is also OFF. This corresponds to discontinuous conduction mode.

The next step is to develop state-space equations for each mode using the state variables defined by

$$x(t) = \begin{bmatrix} i_L(t) & v_o(t) \end{bmatrix}^\top \tag{1}$$

where i_L is the inductor current and v_o is the output voltage (capacitor voltage).

The state-space equations for each mode are defined in Eq. (2).

Mode 1 is realized when Switch S is ON, i_L is positive and increasing, and diode D is not conducting. This mode is represented with Eq. (2a) state equation:

$$\dot{x}(t) = \begin{bmatrix} -\dfrac{R_L}{L} & -\dfrac{1}{L} \\ \dfrac{1}{C} & -\dfrac{1}{RC} \end{bmatrix} x(t) + \begin{bmatrix} -\dfrac{1}{L} \\ 0 \end{bmatrix} v_s(t) \tag{2a}$$

Mode 2 is realized when Switch S is OFF, i_L is positive and decreasing, and diode D is conducting. This mode is represented with the following equation:

$$\dot{x}(t) = \begin{bmatrix} \dfrac{-R_L}{L} & -\dfrac{1}{L} \\ \dfrac{1}{C} & -\dfrac{1}{RC} \end{bmatrix} x(t) + \begin{bmatrix} 0 \\ 0 \end{bmatrix} v_s(t) \tag{2b}$$

Mode 3 is realized when Switch S is OFF, i_L is 0, and diode D is not conducting. This mode is represented with the following equation:

$$\dot{x}(t) = \begin{bmatrix} 0 & 0 \\ 0 & -\dfrac{1}{RC} \end{bmatrix} x(t) + \begin{bmatrix} 0 \\ 0 \end{bmatrix} v_s(t) \tag{2c}$$

2.2 Discrete-Time Model. The forward Euler approximation

$$\frac{x[k+1] - x[k]}{T_s} = f(x[k]) \tag{3}$$

is then used to derive a discrete-time model from the continuous-time model in Eq. (2), where the time increment is defined by T_s.

Where $f(x[k])$ is substituted with the equations in Eq. (2) for each mode. The discrete-time model shares the same three modes as the continuous-time model, and a fourth mode is added to represent the moment the inductor current decreases from a positive value and reaches 0. This instant is defined as τ_1. Hence, the converter operates in four discrete-time modes, depending on the shape of the inductor current and the switch position:

(1) Mode 1 represents the converter when the switch S is ON, and the inductor current is increasing.
(2) Mode 2 is when the switch S is OFF, and the inductor current is decreasing and positive.
(3) Mode 3 is the average of Modes 2 and 4 and includes the moment the inductor current decreases from a positive value to 0, which is defined as τ_1.
(4) Mode 4 is when both switch S and diode D are OFF and the inductor current is 0.

The discrete-time state space matrices for all four modes are included below Eq. (4).

Mode 1 (4a):

$$x[k+1] = \begin{bmatrix} 1 - \dfrac{R_L T_s}{L} & -\dfrac{T_s}{L} \\ \dfrac{T_s}{C} & 1 - \dfrac{T_s}{RC} \end{bmatrix} x[k] + \begin{bmatrix} -\dfrac{T_s}{L} \\ 0 \end{bmatrix} v_s[k] \tag{4a}$$

Mode 2 (4b):

$$x[k+1] = \begin{bmatrix} 1 - \dfrac{R_L T_s}{L} & -\dfrac{T_s}{L} \\ \dfrac{T_s}{C} & 1 - \dfrac{T_s}{RC} \end{bmatrix} x[k] + \begin{bmatrix} 0 \\ 0 \end{bmatrix} v_s[k] \tag{4b}$$

Mode 3 (4*c*):

$$x[k+1] = \begin{bmatrix} 1 - \dfrac{R_L \tau_1}{L} & -\dfrac{\tau_1}{L} \\ \dfrac{\tau_1}{C} & 1 - \dfrac{T_s}{RC} \end{bmatrix} x[k] + \begin{bmatrix} 0 \\ 0 \end{bmatrix} v_s[k] \tag{4c}$$

Mode 4 (4*d*):

$$x[k+1] = \begin{bmatrix} 1 & 0 \\ 0 & 1 - \dfrac{T_s}{RC} \end{bmatrix} x[k] + \begin{bmatrix} 0 \\ 0 \end{bmatrix} v_s[k] \tag{4d}$$

Output:

$$y[k] = \begin{bmatrix} 0 & 1 \end{bmatrix} x[k] \tag{4e}$$

2.3 Kalman Filter Implementation. Model predictive control relies heavily on an accurate dynamic model to predict the system evolution. Additionally, the optimal control action is determined by the initial state of the system, which can be obtained by either direct measurement or through the use of an observer for the states that cannot be directly measured. Direct measurements and observers can suffer from inaccuracies due to measurement errors, noise, and tolerances in the components that are contained within the system model. This is why state estimation, which is the use of past data to determine the most likely value of the state at the current time, becomes a key component for MPC. Similar to our previous work in Ref. [31], the Kalman filter used in this study is derived and configured as follows.

We begin by assuming that both the system and the measurements are affected by disturbances. Accordingly, the system model can be expressed as

$$x[k+1] = A_m x[k] + B_m u + w \tag{5a}$$

$$y[k] = \mathrm{C}x[k] + v \tag{5b}$$

where $x[k]$ denotes the state vector, u the control input, and y the measured output. $x[k+1]$ represents the next state of the system. Note that here the subscript m represents the different modes in Eq. (4) and can be selected from any value $\{1,2,3,4\}$ depending on the switch position and the amplitude of inductor current. A_m, B_m, and C represent the different state-space matrices of the original model in Eq. (4). The term w accounts for process disturbances that affect the system states, whereas v represents measurement noise or sensor inaccuracies. Both w and v are assumed to follow zero-mean Gaussian distributions with covariances Q and R, respectively, i.e., $w \sim N(0,Q)$ and $v \sim N(0,R)$.

By combining noisy measurements with mathematical models of the system, the Kalman filter provides an optimal recursive approach for estimating system states, which consists of two steps. The first step is that the system model and the previous estimated state are used to forecast the next state and its error covariance values (time update). Then, the predicted values are updated using the latest measurement and the computed Kalman gain (measurement update). As new measurements become available, both the Kalman gain and the estimated states are updated continuously, ensuring improved accuracy.

In addition to state estimation, the Kalman filter incorporated into the proposed MPC controller framework also estimates unmeasured disturbances to compensate for load variations and their impact on the system model. During load transients, the resistance R changes, introducing discrepancies between the model and the actual system. To address this, the buck converter is augmented with disturbance states i_e and v_e, which represent the unmodeled effects of load changes on the inductor current and output voltage, respectively [47,48]. The augmented state-space model is given in the following equation:

$$x_{\text{aug}}[k] = \begin{bmatrix} i_L[k] & v_o[k] & i_e[k] & v_e[k] \end{bmatrix}^\top \tag{6}$$

The augmented model in Eq. (7) is used in the prediction step of the Kalman filter.

$$A_{m_{\text{aug}}} = \begin{bmatrix} A_m & \mathbf{0} \\ \mathbf{0} & \boldsymbol{I} \end{bmatrix}, \quad B_{m_{\text{aug}}} = \begin{bmatrix} B_m \\ \mathbf{0} \end{bmatrix}, \quad C_{\text{aug}} = \begin{bmatrix} \boldsymbol{I} & \boldsymbol{I} \end{bmatrix} \tag{7}$$

The Kalman Filter then uses the model to estimate the augmented state in

$$\hat{x}_{\text{aug}} = \hat{x}_{\text{aug}} + K_m(y - C\hat{x}_{\text{aug}}) \tag{8}$$

Again, A_m, B_m, and C represent the different state-space matrices of the original model in Eq. (4), which are used to predict the state $\hat{x}_{\text{aug}}$ and error covariance before measurement y. Entries in matrix K_m are the Kalman gains calculated for the different operating modes. Note that here y is the measurement, while $\hat{x}_{\text{aug}}$ is the estimated stated variable. $\mathbf{0}$ and $\boldsymbol{I}$ are zero and identity matrices respectively.

To enhance estimation performance, the Kalman filter is tuned so that measurement noise has minimal influence by assigning a small value to R. This reflects greater trust in the sensor data. Meanwhile, higher covariance values are used in Q to capture possible process variations and modeling errors. The filter estimates the disturbance terms i_e and v_e, where v_e is fed back to the MPC controller to adjust the reference signal by subtraction, yielding the updated reference as

$$v'_{o,\text{ref}} = v_{o,\text{ref}} - v_e \tag{9}$$

3 Model Predictive Control

3.1 Time-Triggered Enumeration-Based Model Predictive Control. Again, the MPC algorithm illustrated in Fig. 2 starts by generating all possible switching sequences across the prediction horizon of length $N \cdot T_s$, where N is the number of prediction steps and $U(k) = [u(k),\ u(k+1),\ \ldots,\ u(k+N-1)]^\top$. Since the switch status is binary, the total number of possible sequences increases exponentially as 2^N, and evaluating all of them in enumeration-based MPC significantly raises the computational burden. To alleviate this, a move-blocking strategy is implemented [49]. Move blocking divides the prediction horizon into two segments. The first segment consists of N_1 switching steps with sampling period T_s, while the remaining N_2 steps use a longer sampling period by multiplying T_s with a factor n_s. This approach covers the same total prediction horizon with fewer prediction steps, thereby reducing computational burden. As illustrated in Fig. 3, two prediction horizons are compared over the same duration. Without move blocking, the horizon length is $N = 17$, corresponding to a total duration of $17T_s$. With move blocking, the horizon is reduced to $N = 13$, where $N_1 = 9$, $N_2 = 4$, and $n_s = 2$, resulting in the same total length $(9 + (4 \times 2))T_s = 17T_s$. Thus, the computational burden decreases significantly, from $\mathcal{O}(2^{17})$ to $\mathcal{O}(2^{13})$.

Then the MPC solves an optimal control problem (OCP) for each switching sequence, formulated as follows:

$$\min_{U_o} J = \sum_{\ell=k}^{k+N-1} \left(|v_{o,err}[\ell+1|k]| + \lambda_u |\Delta u[\ell|k]| \right. \\ \left. + \lambda_{i_L} |i_{L,err}[\ell|k] \right) \tag{10a}$$

$$\text{s.t. System dynamics Eq. (4)} \tag{10b}$$

The objective (cost) function is defined in Eq. (10*a*). The first term in the objective function penalizes the error between the calculated

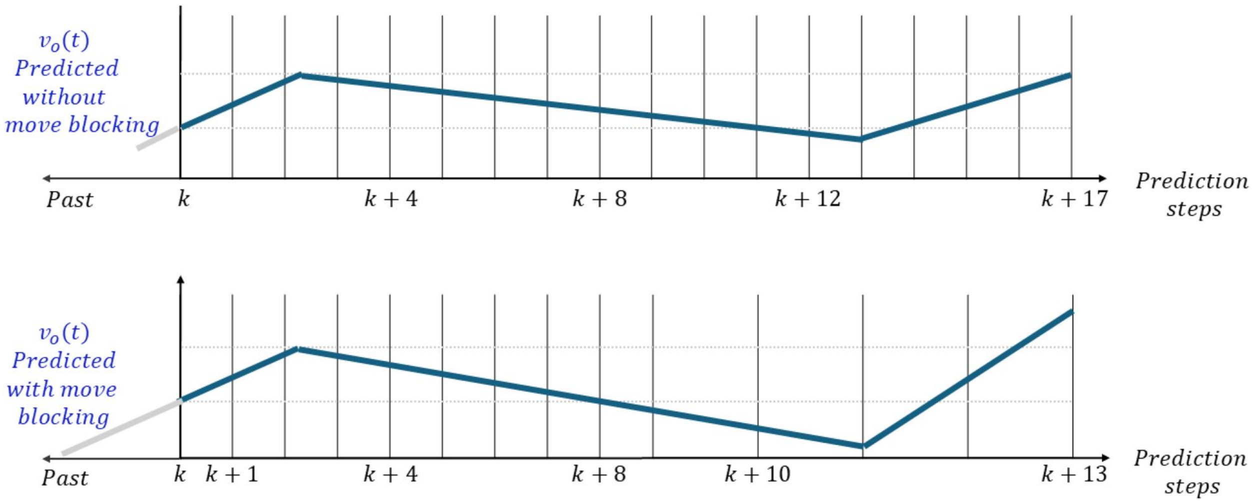

Fig. 3 Prediction horizon move blocking scheme

output voltage and the reference voltage and is found using the following:

$$v_{o,\mathrm{err}}[k] = v_{o,\mathrm{ref}} - v_o[k] \tag{11}$$

The second term in the objective function penalizes the difference between two successive switch states and is calculated using:

$$\Delta u[k] = u[k] - u[k-1] \tag{12}$$

It penalizes the change in the switch state effectively to reduce the switching frequency f_{sw}. This term is manipulated by multiplying it with a weighting factor λ_u, where increasing λ_u generally reduces the switching frequency and setting λ_u to 0 allows the switching frequency to reach $1/(2T_s)$ if $R_L = 0$ and $v_o = 2v_s$ [50]. Weight λ_{i_L} is adjusted to control the influence of the inductor current error, defined as $i_{L,\mathrm{err}}(k) = i_{L,\mathrm{ref}} - i_L(k)$, where $i_{L,\mathrm{ref}}$ is derived using the equation defined in the following equation:

$$v_s i_{L,\mathrm{ref}} = R_L i_{L,\mathrm{ref}}^2 + \frac{v_{\mathrm{ref}}^2}{R} \tag{13}$$

Equation (13) represents that input power equals output power, where we estimate input power by combining the loss across the inductor resistance R_L and the output power. $v_o[k]$ and $i_L[k]$ denote the measured output voltage and inductor current at time k, while $v_o[\ell|k]$ and $i_L[\ell|k]$ represent the predicted states at prediction step ℓ computed at time k. The index k denotes the prediction index, and ℓ denotes the step within the prediction horizon.

At each time-step, the MPC controller evaluates the cost function Eq. (10*a*) for a set of predefined switching sequences U (k). The prediction horizon is defined over a finite horizon $N \in \mathbb{N}^+$ in which the switching sequences are defined:

$$U[k] = \begin{bmatrix} u[k] & u[k+1] & \dots & u[k+N-1] \end{bmatrix}^\top \tag{14}$$

The optimization variable $U[k]$, the input (source) voltage v_s and the current state variable $x[k]$ are then entered into the OCP Eq. (10) where the output voltage trajectory is predicted, and the objective function is evaluated. For real-time implementation, the computational time required to process these sequences is small compared to the sampling time T_s.

The switching sequence with the minimum cost function value is then selected as the optimal switching sequence $U_o[k]$. The first element of the sequence is applied to the switch, S. For time-triggered MPC, this procedure is repeated at the next time step, based on new measurements acquired at the following sampling period T_s.

3.2 Event-Triggered Model Predictive Control.

Event-triggered model predictive control is then adopted to reduce the computational effort required by the enumeration-based TT-MPC. In TT-MPC, the controller evaluates all 2^N switching sequences at every sampling period T_s, which increases computational burden as the prediction horizon N increases. In contrast, ET-MPC solves the OCP only when the voltage tracking objective is no longer satisfied, thereby avoiding unnecessary computations. When an event is triggered, the controller computes the optimal switching sequence U_t and the corresponding state trajectory X_t. The first element of U_t is applied to the main switch S and returned to the controller after a short delay. The delayed switching input and state trajectory are denoted as U_{t1} and X_{t1}, and the event counter t is updated accordingly. Here, t denotes the event counter used in the event-triggered implementation.

At the next sampling period, the counter t is incremented by one sampling period T_s. This counter is used to advance the index k that determines the next switching state. However, when a move blocking scheme is applied, the same switching index may be held for up to n_s sampling periods. To account for this, an index selection matrix T is constructed. The matrix T maps the counter value t to the corresponding index k while incorporating the move blocking structure. An illustrative example of matrix T is provided in Table 2, where $N = 6$, $N_1 = 4$, $n_s = 4$, and $T_s = 5\,\mu$s.

At the next time-step, the optimal state trajectory X_{t1} obtained at the previous event time t_1 is combined with the current output

Table 2 Event-triggered selection of optimal state trajectory and switch state index

<table>
<tr><th>Counter, t</th><th>5 μs</th><th>10 μs</th><th>15 μs</th><th>20 μs</th><th>25 μs</th><th>30 μs</th><th>35 μs</th><th>40 μs</th><th>45 μs</th><th>50 μs</th><th>55 μs</th><th>60 μs</th></tr>
<tr><td>Index, k</td><td>1</td><td>2</td><td>3</td><td>4</td><td colspan="4">5</td><td colspan="4">6</td></tr>
<tr><td>T (k)</td><td>5 μs</td><td>10 μs</td><td>15 μs</td><td>20 μs</td><td colspan="4">40 μs</td><td colspan="4">60 μs</td></tr>
<tr><td>$U_t(k)$</td><td>$U_t[1]$</td><td>$U_t[2]$</td><td>$U_t[3]$</td><td>$U_t[4]$</td><td colspan="4">$U_t[5]$</td><td colspan="4">$U_t[6]$</td></tr>
<tr><td>$X(k)$</td><td>X [1]</td><td>X [2]</td><td>X [3]</td><td>X [4]</td><td colspan="4">X [5]</td><td colspan="4">X [6]</td></tr>
</table>

voltage measurement v_o to evaluate the event condition. The event signal e is determined according to the following criterion:

$$e = \begin{cases} 1, & \text{if } ||X_{t1}[2,k] - v_o|| > \delta \text{ or } k > k_{\max} \\ 0, & \text{Otherwise} \end{cases} \tag{15}$$

where δ denotes the trigger threshold and specifies the deviation between the measured output voltage v_o and the predicted state $X_{t1}(2, k)$ corresponding to the optimal trajectory.

An event is activated when $e = 1$, letting the controller solve the OCP Eq. (10). An event is also triggered when the index reaches $k_{\max}$, which denotes the maximum number of elements permitted in the switching sequence. In either case, a new optimal state trajectory and switching sequence are computed and sent back to the controller. When $e = 0$, the controller applies the next switching action from the previously computed optimal sequence U_{t1}, and no optimization over the 2^N switching sequences is required [51]. Specifically, each triggered event corresponds to a full reevaluation of the optimal control problem Eq. (10). When $e = 1$, the controller performs a complete enumeration-based MPC optimization, where all admissible switching sequences over the prediction horizon are evaluated. When $e = 0$, no optimization is executed; the controller only performs trigger evaluation, trajectory index updating, and direct retrieval of the previously computed switching action. Therefore, the event frequency reflects the number of full MPC optimizations.

The event-triggered control algorithm is described in Algorithm 1 and in the flowchart in Fig. 4, where J represents the cost function in Eq. (10a).

Algorithm 1 Event-Triggered MPC Algorithm

```
procedure: ETMPC (u, U_t1, X_t1, t, i_l, v_o, v_s)
    J*(k) = ∞;
    t ← t + T_s
    k ← select k from T using t see Table 2
    e ← compute Eq. (15);
if e = 1 then
    t ← 0
    for all U over N do
        J = 0
        for ℓ = k to k + N − 1 do
            x(ℓ + 1) ← compute from Eqs. (4), (6), and (7)
            J ← compute from Eq. (10)
        end
        if J < J*(k) then
            J*(k) = J, u = U(1)
        end
    end
    U_t ← U
    X_t ← x
end
if e = 0 then
    u ← U_t1(k)
    U_t ← U_t1
    X_t ← X_t1
end
return u, t, U_t, X_t
end procedure
```

The triggering condition in Eq. (15) is introduced to reduce the online computational burden while maintaining satisfactory closed-loop performance. Between two consecutive events, the controller applies the previously computed optimal switching sequence and monitors the deviation between the measured output voltage and the predicted trajectory. As long as this deviation remains below the threshold δ, the converter operates close to the nominal MPC-predicted behavior. When the deviation exceeds δ, a new MPC optimization is executed to update the switching sequence. As a result, the output voltage tracking error remains bounded and can be regulated through the choice of δ, reflecting the tradeoff between computational effort and control performance. Along the same logic, excessive triggering can be avoided through the tuning of δ.

As this paper focuses on the algorithmic development and numerical validation, readers are referred to Refs. [52,53] for stability and Zeno behavior in ET-MPC.

4 Implementation and Simulation Results

Figure 4 illustrates the simulation test environment used in this study, including the buck converter plant, the ET-MPC controller, and the Kalman filter for state and disturbance estimation. Compared with our former work on the boost converter [31], one modification is made with regard to the estimation of the inductor current because the inductor is connected directly to the output capacitor C and load resistor R. As an estimate, the inductor current can be assumed to be equal to the load current:

$$i_{L,\text{ref}} = \frac{v_{o,\text{ref}}}{R} \tag{16}$$

Time-triggered model predictive control is implemented with the event-trigger threshold δ being set to 0.

The parameters used in the simulation are listed in Table 3. In particular, a prediction horizon $N = 8$ is selected. Unlike the case of a boost converter, the performance of the system is evaluated during startup and step changes in the input voltage, reference voltage, and load.

4.1 Buck Converter Startup. During startup, the reference voltage is applied at 0.1 ms. This delay is applied in order to observe the startup sequence with more clarity. The results from both TT-MPC and ET-MPC controllers, as shown in Figs. 5 and 6, show that the buck converter experiences an overshoot at the output before returning to regulation at 3 ms during startup. This is due to switch S going to the *ON* state for a duration long enough to allow an inrush of current into the output capacitor and raise the output voltage to $v_{o,\text{ref}} = 5$ V. The switch then turns *OFF*. During this scenario, the inductor current finds an alternate path through the diode D by forward biasing the diode and allowing the current to continue to flow to the output, which in this case causes the capacitor to charge up to a higher voltage, approximately 7 V. For the remainder of the duration during which switch S is *OFF* the output capacitor voltage drops as it discharges through the load resistor R to 5 V. When this happens, the controller begins to actuate the switch, and normal conversion takes place, allowing the buck converter to reach regulation.

In order to avoid overshoot, a Soft-Start (*SS*) scheme is applied to the converter to ramp the reference voltage up. The operation of the TT-MPC and ET-MPC without and with soft-start is compared in Figs. 5 and 6, respectively. Table 4 summarizes important attributes during startup for both TT-MPC and ET-MPC. Both formulations exhibit similar overshoot and startup times. However, the key difference between the methods is the peak inductor current, which is different as a result of the switching frequency. Since ET-MPC results in a lower switching frequency of 55 kHz when compared with TT-MPC for 125 kHz, the inductor peak current is higher during the startup of ET-MPC. An additional observation is the reduction in computational burden achieved by utilizing the event-trigger formulation, in which the OCP is triggered approximately 10% of the time once the converter reaches steady-state.

4.2 Steady-State Operation. The buck converter is evaluated for different steady-state conditions and trigger thresholds that are listed in Table 5. Since the optimization problem solved at each event has a fixed structure and prediction horizon, the computational effort is proportional to the number of optimization runs; therefore, the event frequency is used as a normalized metric to quantify the computational burden. The table includes the event frequency, T.E. and output ripple, where the tracking error is calculated using

$$\text{T.E.} = \sqrt{\frac{\sum_{i=1}^{n}\left(v_o[i] - v_{o,\text{ref}}[i]\right)^2}{n}} \tag{17}$$

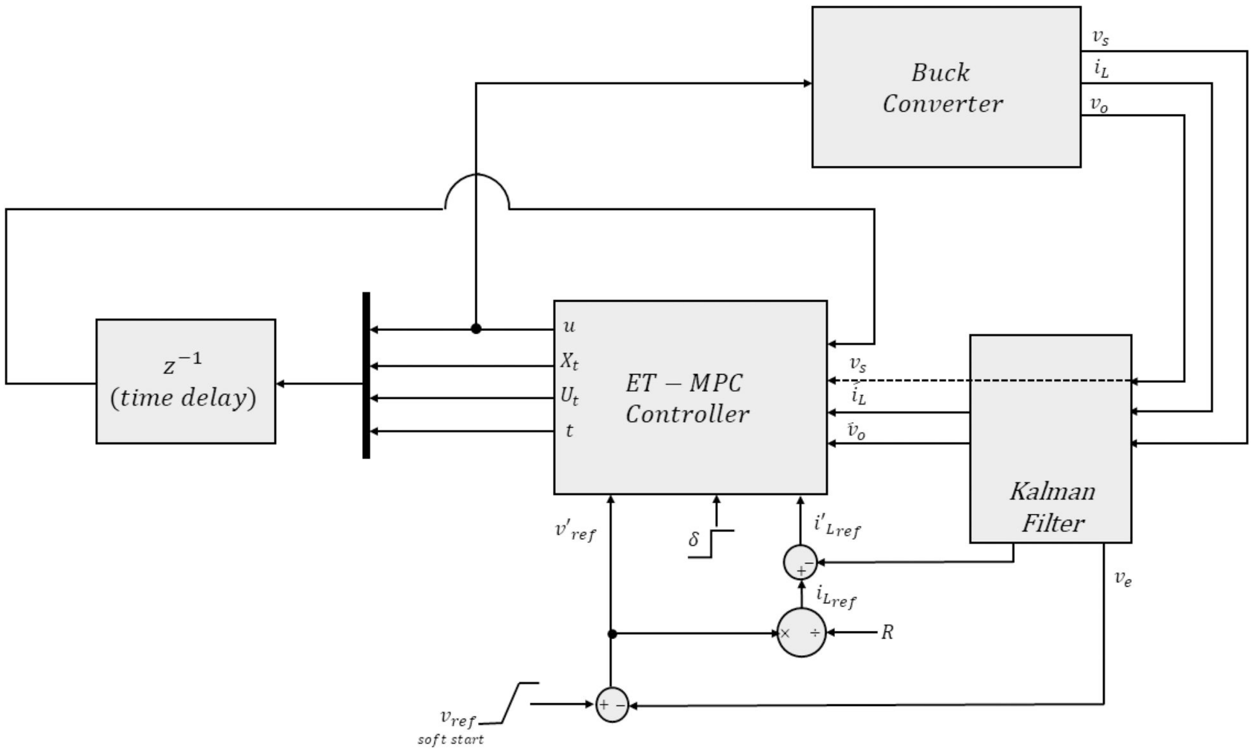

Fig. 4 Buck converter ET-MPC implementation block diagram

Table 3 Simulation parameters – buck converter with Kalman filter

Converter and controller parameter	Value
Input Voltage (v_s)	16 V
Output voltage ($v_{o,\text{ref}}$)	5 V
Inductor (L)	100 μH
Inductor DC resistance (R_L)	0.3Ω
Output capacitance (C)	220 μF
Load resistance (R)	36Ω → 18Ω
Sampling period (T_s)	2.5 μs
Prediction horizon (N)	8
N_1	4
Move blocking coefficient (n_s)	4
Allowable optimal switching elements ($k_{\max}$)	7
Switching – weighting factor (λ_u)	0.05
Inductor current – weighting factor (λ_{iL})	0.05
Minimum event frequency ($f_{\min-\text{ET}}$)	6.25%

As can be seen, increasing the trigger threshold δ significantly reduces the computational effort of the controller during steady-state operation. Additionally, increasing δ also increases the output voltage ripple and peak inductor current, and reduces the switching frequency. The number of events increases as the difference between the input and output voltage increases.

When events are not triggered, we are able to skip the optimization problem for up to 16 time steps since the last event is triggered ($N_1 = 4, k_{\max} = 7, n_s = 4 \rightarrow 4 + ((7-4) \times 4) = 16$).

The minimum event frequency possible for the buck converter is found to be 6.25% computed by

$$f_{\min-\text{ET}} = \begin{cases} \dfrac{1}{(N_1 + (k_{\max} - N_1)n_s)} & \text{if } k_{\max} \geq N_1 \\ \dfrac{1}{k_{\max}} & \text{if } k_{\max} < N_1 \end{cases} \tag{18}$$

Furthermore, the minimum event average frequency is found to be 6.65% when the input voltage is 12 V and the output voltage reference is 3.3 V. The computational savings in this scenario are realized by reducing the number of times the OCP is triggered by 93%.

To evaluate the harmonic performance of the proposed ET-MPC, Table 6 summarizes the dominant ripple frequency, ripple RMS, total waveform distortion (TWD), and peak-to-peak ripple under steady-state operation at $v_s = 16$ V and $v_{o,\text{ref}} = 5$ V. TWD is defined as

$$\text{TWD} = \frac{\sqrt{V_{\text{rms}}^2 - V_1^2}}{V_1} \times 100\% \tag{19}$$

where V_{rms} is the total ripple RMS and V_1 is the RMS of the dominant spectral component. As δ increases, the dominant ripple frequency decreases from 9.00 kHz to 3.33 kHz, consistent with the reduced switching activity reported in Table 5. The ripple RMS and TWD both increase monotonically with δ, from 16.44 mV and 63.17% for TT-MPC to 52.62 mV and 157.15% at $\delta = 0.025$, confirming that the event-triggered strategy introduces additional waveform distortion as a tradeoff for the significant reduction in computational effort.

4.3 Step Changes in the Output Reference Voltage. Figure 7 shows the results for a step-up in reference voltage from 3.3 V to 5 V. The reference voltage is applied with a slew rate approximately equal to 4 V/ms. In both formulations, the inductor current and switching frequency increase during the transition. The corresponding quantitative results under different event thresholds are summarized in Table 7.

Next, the output voltage reference is stepped down from 5 V to 3.3 V at 10 ms. The response of the converter using both TT-MPC and ET-MPC methods is illustrated in Fig. 8. Both control methods enable the converter to reach regulation within 3 ms, with the latter achieving comparable performance while requiring significantly fewer computations. On average, the OCP is only triggered 9% of the time duration when compared to TT-MPC. Another operation occurs during the step down, in which the inductor current goes to zero, allowing the capacitor to discharge into the load to reduce the output voltage to the new reference voltage.

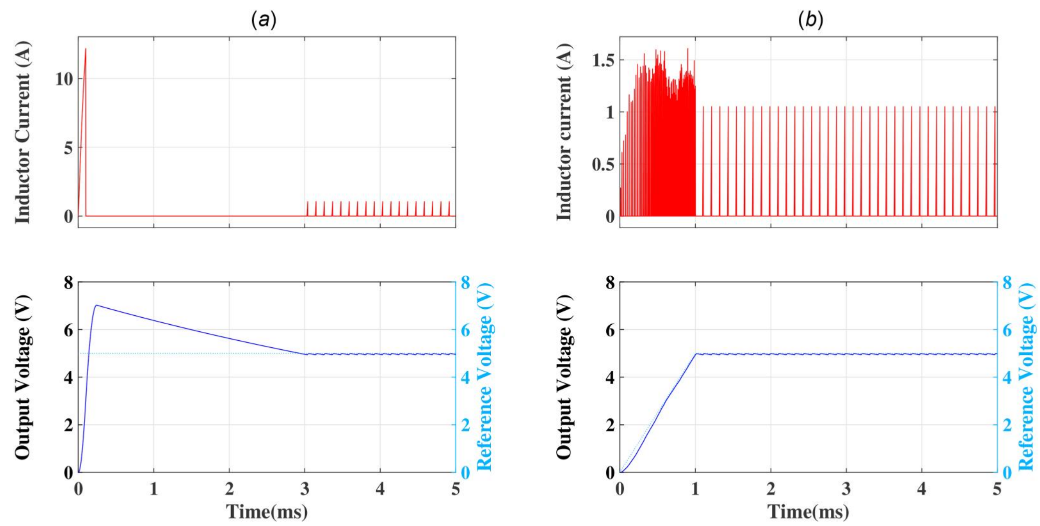

Fig. 5 Buck converter startup without (*a*) and with soft-start (*b*) (TT-MPC)

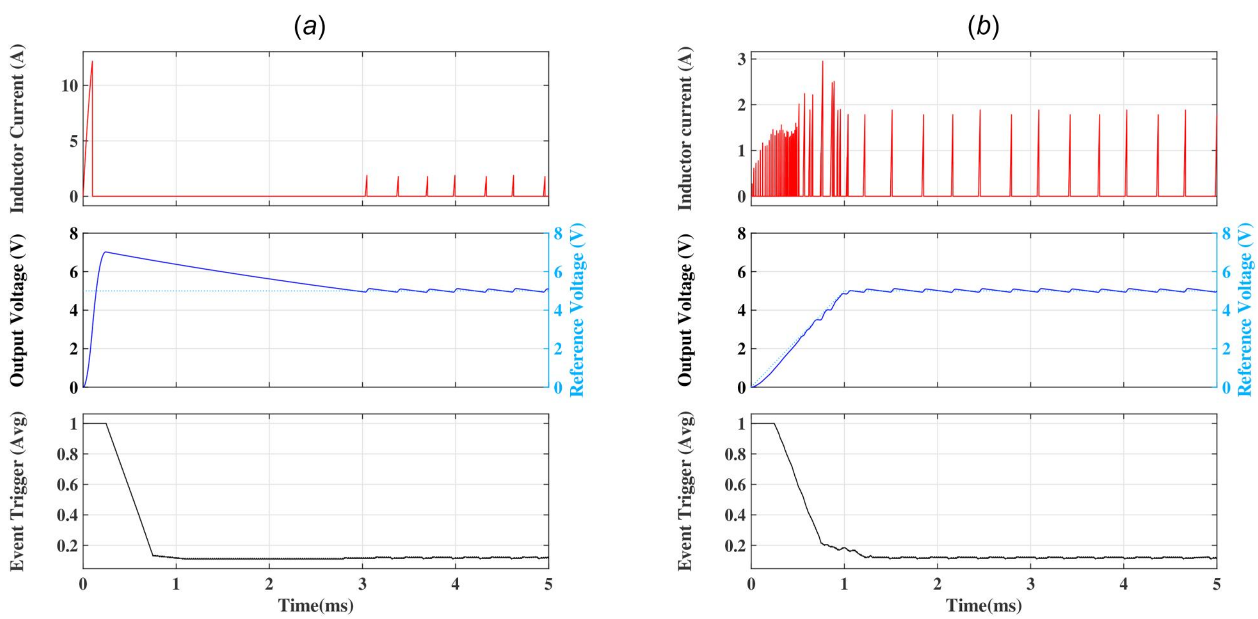

Fig. 6 Buck converter startup without (*a*) and with soft-start (*b*) (ET-MPC - δ=0.025)

Table 4 Startup attributes summary

	TT-MPC		ET-MPC	
Soft-start (SS) implementation	No SS	With SS	No SS	With SS
Overshoot (%)	40%	0%	40%	0%
Peak inductor current (A)	12.2 A	1.8 A	12.2 A	3 A
Maximum f_{sw}(kHz) during startup	NA	125 kHz	NA	55 kHz

4.4 Step Change in the Input Voltage (Line Transient). Results for both TT-MPC and ET-MPC for a line transient case are shown in Fig. 9. The input voltage is stepped down from 16 V to 12 V at 10 ms after steady-state operation with $v_{o,\text{ref}}$ set to 5 V. The line transient response of the converter in both controllers is similar, showing that the converter is able to maintain the output voltage within regulation. The event frequency decreases during the transient is maintained at approximately 12%. An additional note can be made about the TT-MPC controller, where it experiences a lower switching frequency as the input voltage decreases.

4.5 Response to Load Transients. The load resistance R is reduced from 36Ω to 18Ω to simulate an increase in load demand. The Kalman filter is used to estimate the measured inductor current, output voltage and disturbance variables i_e and v_e which are fed back to the controller to adjust the inductor current and output voltage references and compensate for the load disturbance.

The output reference voltage is set to 5 V and the input voltage is set to 16 V. The covariance matrices for process noise Q and measurement noise R are assigned the values in the following equation:

$$Q = \begin{bmatrix} 0.1 & 0 & 0 & 0 \\ 0 & 0.1 & 0 & 0 \\ 0 & 0 & 50 & 0 \\ 0 & 0 & 0 & 50 \end{bmatrix}, \quad R = \begin{bmatrix} 1 & 0 \\ 0 & 1 \end{bmatrix} \tag{20}$$

Table 5 Event-trigger impact on steady-state operation – results summary

Event frequency: Steady-state conditions	$\delta = 0.00$	$\delta = 0.015$	$\delta = 0.025$	$\delta = 0.035$
$v_s = 12\,\text{V}, v_o = 3.3\,\text{V}$	100%	10.93%	7.95%	6.65%
$v_s = 12\,\text{V}, v_o = 5\,\text{V}$	100%	18.2%	11.33%	7.48%
$v_s = 16\,\text{V}, v_o = 3.3\,\text{V}$	100%	12.34%	8.16%	6.84%
$v_s = 16\,\text{V}, v_o = 5\,\text{V}$	100%	19.80%	11.98%	9.13%
Tracking error (V): Steady-state conditions	$\delta = 0.00$	$\delta = 0.015$	$\delta = 0.025$	$\delta = 0.035$
$v_s = 12\,\text{V}, v_o = 3.3\,\text{V}$	0.034 V	0.033 V	0.047 V	0.064 V
$v_s = 12\,\text{V}, v_o = 5\,\text{V}$	0.066 V	0.053 V	0.051 V	0.053 V
$v_s = 16\,\text{V}, v_o = 3.3\,\text{V}$	0.033 V	0.029 V	0.052 V	0.053 V
$v_s = 16\,\text{V}, v_o = 5\,\text{V}$	0.035 V	0.039 V	0.059 V	0.050
Output ripple [Vp-p]: Steady-state conditions	$\delta = 0.00$	$\delta = 0.015$	$\delta = 0.025$	$\delta = 0.035$
$v_s = 12\,\text{V}, v_o = 3.3\,\text{V}$	0.048	0.116	0.161	0.219
$v_s = 12\,\text{V}, v_o = 5\,\text{V}$	0.086	0.135	0.171	0.210
$v_s = 16\,\text{V}, v_o = 3.3\,\text{V}$	0.060	0.101	0.163	0.163
$v_s = 16\,\text{V}, v_o = 5\,\text{V}$	0.055	0.128	0.193	0.165

Table 6 Harmonic performance summary under steady-state operation (v_s=16 V, $v_{o,\text{ref}}$=5 V)

Metric	TT-MPC	ET-MPC ($\delta = 0.015$)	ET-MPC ($\delta = 0.025$)
Dominant ripple frequency (kHz)	9.00	4.12	3.33
Ripple RMS (mV)	16.44	38.26	52.62
TWD (%)	63.17	142.08	157.15
Output ripple, peak-to-peak (mV)	55.0	128.0	193.0

The covariance matrices Q and R are selected based on the relative confidence in the system model, disturbance dynamics, and measurements. Specifically, small covariance values are assigned

Table 7 Voltage reference converter response for different event thresholds

	$\delta = 0.00$	$\delta = 0.025$
$v_{o,\text{ref}} = 3.3\,\text{V} \rightarrow 5\,\text{V}, v_s = 16\,\text{V}$		
Transient time (ms)	0.5 ms	0.5 ms
Event frequency	100%	23.5%
$v_{o,\text{ref}} = 5\,\text{V} \rightarrow 3.3\,\text{V}, v_s = 16V$		
Transient time (ms)	3.5 ms	3.5 ms
Event frequency	100%	9%

to the physical states to reflect their dynamics, while significantly larger values are used for the disturbance-related states to enable fast adaptation to load variations and modeling mismatch; the measurement noise covariance R is set to the identity matrix, indicating moderate confidence in the voltage and current measurements. In practice, the Kalman filter exhibits robust convergence behavior, where moderate variations in Q and R mainly affect transient estimation accuracy without compromising the closed-loop MPC performance [15,54].

The results comparing the TT-MPC and ET-MPC controllers are reported in Fig. 10. It can be seen that both controllers are able to regulate the output voltage with no undershoot.

The ET-MPC controller is also evaluated for different event-trigger thresholds. The waveforms in Fig. 11 illustrate a clear trend that increasing the event-trigger threshold δ leads to lower event occurrences and switching frequencies, while the peak inductor current and the output voltage ripple become larger. Despite these variations, the transient responses in all cases remain favorable, and the converter successfully maintains voltage regulation as the load current increases.

The results presented in this paper are based on simulation results, which represent a limitation with respect to real-time experimental validation. Nevertheless, the proposed ET-MPC framework is developed with real-time implementation in mind and is suitable for embedded platforms such as digital signal processors or micro-controller units. Since the enumeration-based optimization is executed only at event instants with a fixed and small prediction horizon, the computational burden is significantly reduced, making the approach feasible for the sampling period considered in this study.

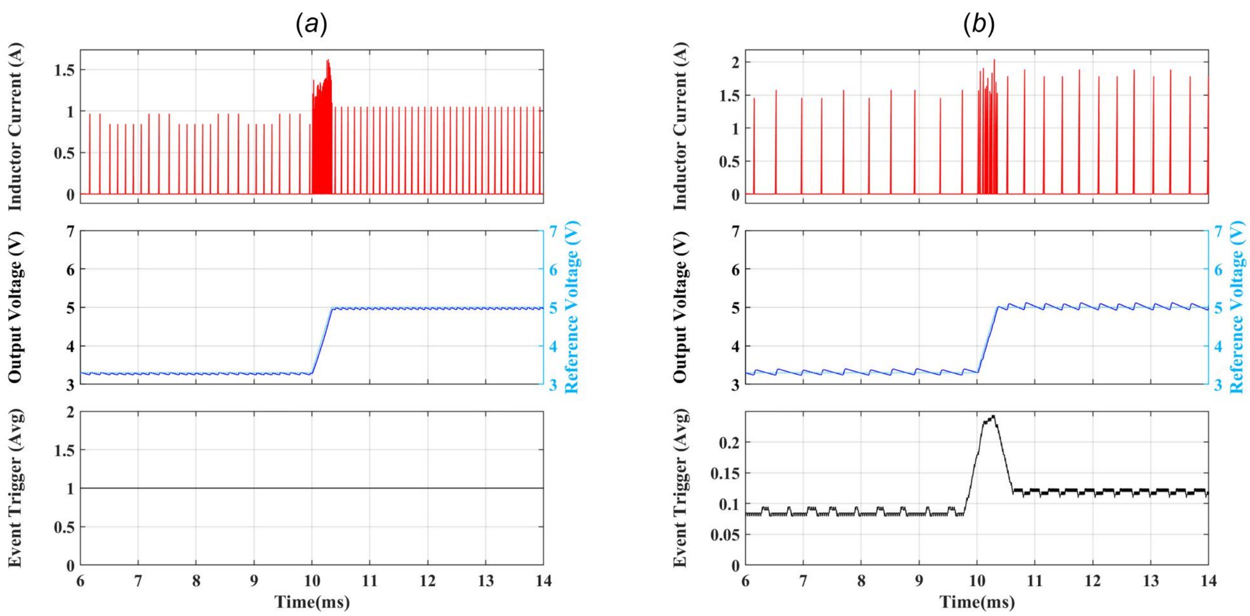

Fig. 7 Reference voltage step-up from 3.3 V to 5 V (TT-MPC and ET-MPC): (*a*) reference step-up (TT-MPC) and (*b*) reference step-up (ET-MPC $\delta = 0.025$)

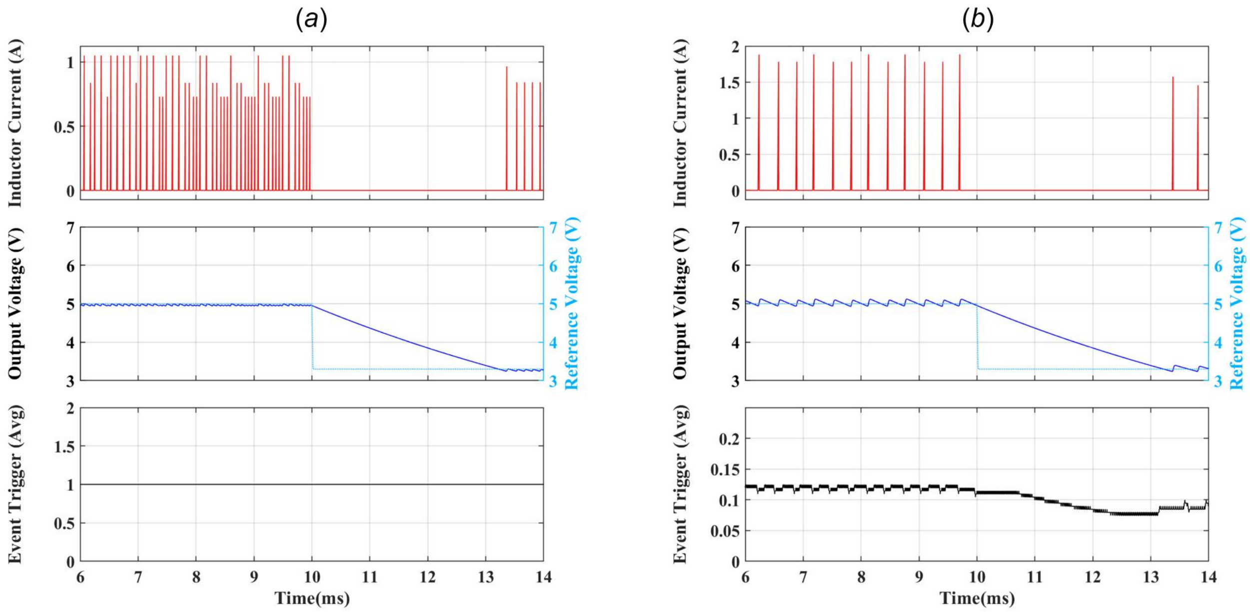

Fig. 8 **Reference voltage step-down from 5 V to 3.3 V (TT-MPC and ET-MPC) : (*a*) reference step-up (TT-MPC) and (*b*) reference step-up (ET-MPC $\delta = 0.025$)**

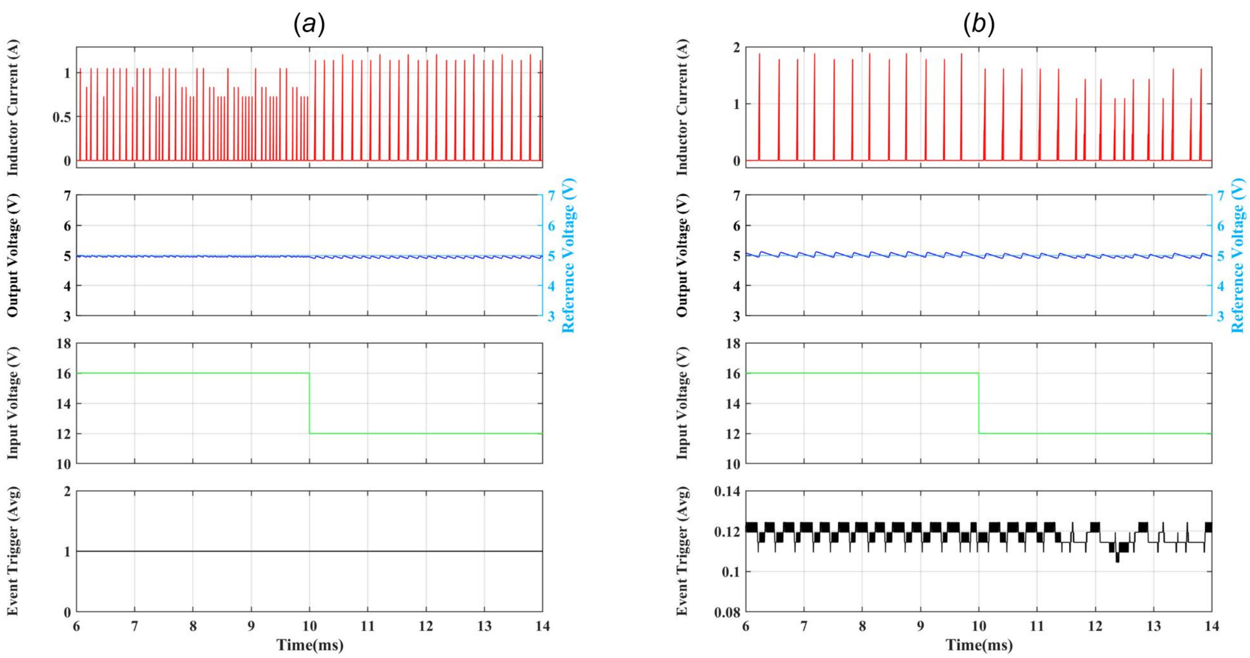

Fig. 9 **Input voltage step-down from 16 V to 12 V (TT-MPC and ET-MPC (δ=0.025)): (*a*) input voltage step-down (TT-MPC) and (*b*) input voltage step-down (ET-MPC $\delta = 0.025$)**

5 Conclusion

This paper presents an ET-MPC strategy for a DC–DC buck converter to reduce computational effort while maintaining fast transient and steady-state performance. A four-mode discrete-time model is established, and a Kalman filter is incorporated to enhance state estimation and compensate for load disturbances. The proposed output-error based triggering mechanism allows the controller to perform online optimization only when the voltage deviation exceeds a threshold, resulting in up to a 94% reduction in computational effort at $\delta = 0.035$. Simulation results confirm that the ET-MPC achieves similar regulation quality to the time-triggered MPC with faster recovery, lower switching frequency, and acceptable current peaks. The results demonstrate that the proposed ET-MPC framework provides an efficient and reliable approach for real-time control of power converters under varying operating conditions. Future work will focus on experimental validation of the proposed approach on a real-time hardware platform. Subsequently, tradeoffs between prediction horizon length and control performance will be examined, along with systematic tuning of the weighting factors and event-trigger threshold to achieve consistent switching frequency under both steady-state and transient operating conditions. In addition, comparisons with alternative event-triggered control strategies, such as event-triggered sliding mode control, will be considered in future experimental studies.

Conflict of Interest

There are no conflicts of interest.

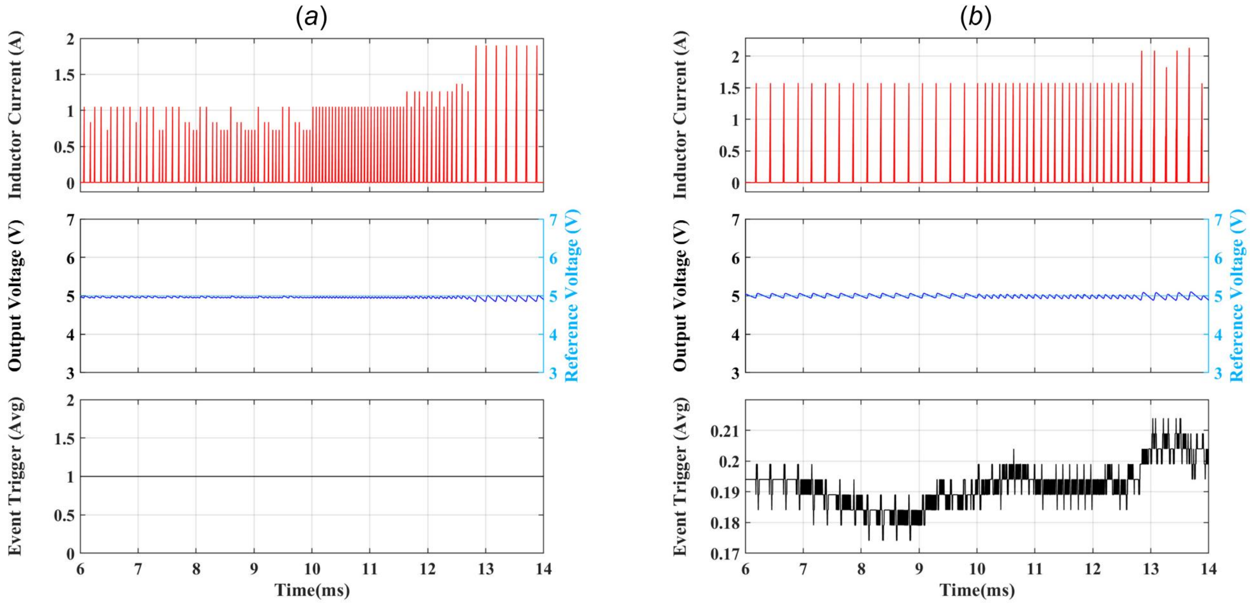

Fig. 10 Load transient for TT-MPC and ET-MPC (δ=0.015) – buck converter: (*a*) load transient (36Ω → 18Ω (TT-MPC)) and (*b*) load transient (36Ω → 18Ω (ET-MPC δ = 0.015))

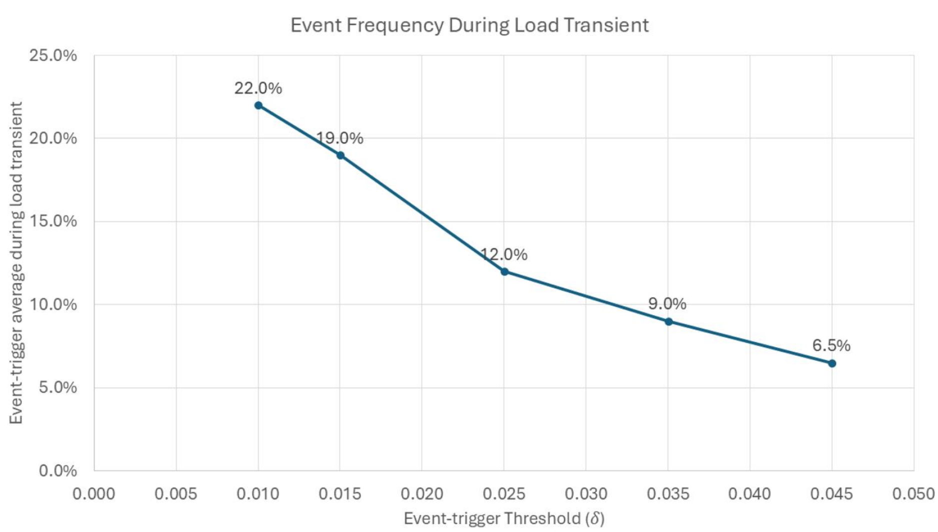

Fig. 11 Average event frequency during load transient

Funding Data

- National Science Foundation (Award Nos. 2237317 and 2430374; Funder ID: 10.13039/100000084).

Data Availability Statement

The datasets generated and supporting the findings of this article are obtainable from the corresponding author upon reasonable request.

References

[1] Safayatullah, M., Elrais, M. T., Ghosh, S., Rezaii, R., and Batarseh, I., 2022, "A Comprehensive Review of Power Converter Topologies and Control Methods for Electric Vehicle Fast Charging Applications," IEEE Access, **10**, pp. 40753–40793.

[2] Vazquez, S., Rodriguez, J., Rivera, M., Franquelo, L. G., and Norambuena, M., 2017, "Model Predictive Control for Power Converters and Drives: Advances and Trends," IEEE Trans. Ind. Electron., **64**(2), pp. 935–947.

[3] Ansari, S., Chandel, A., and Tariq, M., 2021, "A Comprehensive Review on Power Converters Control and Control Strategies of AC/DC Microgrid," IEEE Access, **9**, pp. 17998–18015.

[4] Hu, J., Shan, Y., Cheng, K. W., and Islam, S., 2022, "Overview of Power Converter Control in Microgrids—Challenges, Advances, and Future Trends," IEEE Trans. Power Electron., **37**(8), pp. 9907–9922.

[5] Kouro, S., Cortés, P., Vargas, R., Ammann, U., and Rodríguez, J., 2009, "Model Predictive Control—a Simple and Powerful Method to Control Power Converters," IEEE Trans. Ind. Electron., **56**(6), pp. 1826–1838.

[6] Aguilar-Ibanez, C., Moreno-Valenzuela, J., Garcia-Alarcon, O., Martinez-Lopez, M., Acosta, J. A., and Suarez-Castanon, M. S., 2021, "Pi-Type Controllers and σ–δ Modulation for Saturated DC-DC Buck Power Converters," IEEE Access, **9**, pp. 20346–20357.

[7] Chen, Z., 2012, "PI and Sliding Mode Control of a Cuk Converter," IEEE Trans. Power Electron., **27**(8), pp. 3695–3703.

[8] Beerten, J., and Belmans, R., 2013, "Analysis of Power Sharing and Voltage Deviations in Droop-Controlled DC Grids," IEEE Trans. Power Syst., **28**(4), pp. 4588–4597.

[9] Lee, C.-T., Chu, C.-C., and Cheng, P.-T., 2013, "A New Droop Control Method for the Autonomous Operation of Distributed Energy Resource Interface Converters," IEEE Trans. Power Electron., **28**(4), pp. 1980–1993.
[10] Zhang, X., Wang, Y., Yu, C., Guo, L., and Cao, R., 2016, "Hysteresis Model Predictive Control for High-Power Grid-Connected Inverters With Output LCL Filter," IEEE Trans. Ind. Electron., **63**(1), pp. 246–256.
[11] Stanojev, O., Markovic, U., Aristidou, P., Hug, G., Callaway, D., and Vrettos, E., 2022, "MPC-Based Fast Frequency Control of Voltage Source Converters in Low-Inertia Power Systems," IEEE Trans. Power Syst., **37**(4), pp. 3209–3220.
[12] Richter, S., Mariéthoz, S., and Morari, M., 2010, "High-Speed Online MPC Based on a Fast Gradient Method Applied to Power Converter Control," 2010 American Control Conference, Baltimore, MD, June 30–July 2, pp. 4737–4743.
[13] Wang, B., Huang, J., Wen, C., Rodriguez, J., Garcia, C., Gooi, H. B., and Zeng, Z., 2021, "Event-Triggered Model Predictive Control for Power Converters," IEEE Trans. Ind. Electron., **68**(1), pp. 715–720.
[14] Kouvaritakis, B., and Cannon, M., 2016, *Model Predictive Control*, Springer International Publishing, Cham, Switzerland.
[15] Rawlings, J. B., Mayne, D. Q., and Diehl, M., 2020, *Model Predictive Control: Theory, Computation, and Design*, Nob Hill Publishing, Madison, WI, Vol. 2.
[16] Cortés, P., Kouro, S., La Rocca, B., Vargas, R., Rodriguez, J., Leon, J. I., Vazquez, S., and Franquelo, L. G., 2009, "Guidelines for Weighting Factors Design in Model Predictive Control of Power Converters and Drives," IEEE International Conference on Industrial Technology, Churchill, VIC, Australia, Feb. 10–13, pp. 1–7.
[17] Karamanakos, P., Liegmann, E., Geyer, T., and Kennel, R., 2020, "Model Predictive Control of Power Electronic Systems: Methods, Results, and Challenges," IEEE Open J. Ind. Appl., **1**, pp. 95–114.
[18] Di Salvo, S. R., Leuzzi, R., Tresca, G., Anglani, N., and Zanchetta, P., 2022, "Self-Tuning Finite-State Model Predictive Control With Grid Impedance Estimation in a Grid-Tied Inverter," IEEE Energy Conversion Congress and Exposition (ECCE), Detroit, MI, Oct. 9–13, pp. 1–7.
[19] Ding, W., Faraji, F., Jayan, V., Zuo, W., Ghias, A. M., and Cha, H., 2022, "Finite Control Set Model Predictive Control for Five-Level Modified Active Nested Neutral Point Clamped Converter," IEEE Energy Conversion Congress and Exposition (ECCE), Detroit, MI, Oct. 9–13, pp. 1–5.
[20] Liu, X., Qiu, L., Wu, W., Ma, J., Fang, Y., Peng, Z., Wang, D., and Rodríguez, J., 2023, "Event-Triggered ESO-Based Robust MPC for Power Converters," IEEE Trans. Ind. Electron., **70**(2), pp. 2144–2152.
[21] Dang, F., Chen, D., Chen, J., and Li, Z., 2024, "Event-Triggered Model Predictive Control With Deep Reinforcement Learning for Autonomous Driving," IEEE Trans. Intell. Veh., **9**(1), pp. 459–468.
[22] Lin, H., Liu, J., Shen, X., Yin, Y., Leon, J. I., Franquelo, L. G., and Wu, L., 2021, "Event-Triggered Continuous Control Set-Model Predictive Control for Three-Phase Power Converters," IECON 2021–47th Annual Conference of the IEEE Industrial Electronics Society, Toronto, ON, Canada, Oct. 13–16, pp. 1–6.
[23] Zhou, Z., Rother, C., and Chen, J., 2023, "Event-Triggered Model Predictive Control for Autonomous Vehicle Path Tracking: Validation Using CARLA Simulator," IEEE Trans. Intell. Veh., **8**(6), pp. 3547–3555.
[24] Flessner, D., Chen, J., and Xiong, G., 2024, "Reinforcement Learning-Based Event-Triggered Active Battery Cell Balancing Control for Electric Vehicle Range Extension," Electronics, **13**(5), p. 990.
[25] Flessner, D., and Chen, J., 2025, "Reinforcement Learning-Based Event-Triggered Model Predictive Control for Electric Vehicle Active Battery Cell Balancing," ASME Lett. Dyn. Syst. Control, **5**(2), p. 024502.
[26] Chakrabarty, A., Zavitsanou, S., Doyle, F. J., and Dassau, E., 2018, "Event-Triggered Model Predictive Control for Embedded Artificial Pancreas Systems," IEEE Trans. Biomed. Eng., **65**(3), pp. 575–586.
[27] Zhou, Z., Chen, J., Tao, M., Zhang, P., and Xu, M., 2023, "Experimental Validation of Event-Triggered Model Predictive Control for Autonomous Vehicle Path Tracking," IEEE International Conference on Electro Information Technology (eIT), Romeoville, IL, May 18–20, pp. 35–40.
[28] Chen, Q., Wang, B., Peng, W., and Rodriguez, J., 2021, "Cost Function Decoupling of FS-MPC for Power Converter Using Event-Triggered Mechanism," IEEE International Conference on Predictive Control of Electrical Drives and Power Electronics (PRECEDE), Jinan, China, Sept. 18–20, pp. 104–108.
[29] Badawi, R., and Chen, J., 2022, "Enhancing Enumeration-Based Model Predictive Control for DC-DC Boost Converter With Event-Triggered Control," European Control Conference (ECC), London, UK, July 12–15, pp. 723–728.
[30] Badawi, R., and Chen, J., 2022, "Performance Evaluation of Event-Triggered Model Predictive Control for Boost Converter," IEEE Vehicle Power and Propulsion Conference (VPPC), Merced, CA, Nov. 1–4, pp. 1–6.
[31] Badawi, R., and Chen, J., 2024, "Event-Triggered Boost Converter Model Predictive Control With Kalman Filter," Syst. Sci. Control Eng., **12**(1), p. 2438866.
[32] Filter, K., 2024, "Simultaneous Cell State Estimation Via Dense Adaptive Extended," Ph.D. thesis, Oakland University, Rochester, MI.
[33] Khodarahmi, M., and Maihami, V., 2023, "A Review on Kalman Filter Models," Arch. Comput. Methods Eng., **30**(1), pp. 727–747.
[34] Ali, J. M., Hoang, N. H., Hussain, M. A., and Dochain, D., 2015, "Review and Classification of Recent Observers Applied in Chemical Process Systems," Comput. Chem. Eng., **76**, pp. 27–41.
[35] Auger, F., Hilairet, M., Guerrero, J. M., Monmasson, E., Orlowska-Kowalska, T., and Katsura, S., 2013, "Industrial Applications of the Kalman Filter: A Review," IEEE Trans. Ind. Electron., **60**(12), pp. 5458–5471.
[36] Vinodh, K. E., Jovitha, J., and Ayyappan, S., 2013, "Comparison of Four State Observer Design Algorithms for MIMO System," Arch. Control Sci., **23**(2), pp. 243–256.
[37] Feng, S., Li, X., Zhang, S., Jian, Z., Duan, H., and Wang, Z., 2023, "A Review: State Estimation Based on Hybrid Models of Kalman Filter and Neural Network," Syst. Sci. Control Eng., **11**(1), p. 2173682.
[38] Erickson, R. W., and Maksimovic, D., 2007, *Fundamentals of Power Electronics*, Springer Science & Business Media, New York.
[39] Mohan, N., Undeland, T. M., and Robbins, W. P., 2003, *Power Electronics: Converters, Applications, and Design*, John Wiley & Sons, Hoboken, NJ.
[40] Ntogramatzidis, L., Cuoghi, S., Ricco, M., Mandrioli, R., and Grandi, G., 2023, "A Novel MIMO Control for Interleaved Buck Converters in EV DC Fast Charging Applications," IEEE Trans. Control Syst. Technol., **31**(4), pp. 1892–1900.
[41] Baharudin, N., Mansur, T., Hamid, F., Ali, R., and Misrun, M., 2018, "Performance Analysis of DC-DC Buck Converter for Renewable Energy Application," J. Phys.: Conf. Ser., **1019**, p. 012020.
[42] Liou, W.-R., Yeh, M.-L., and Kuo, Y. L., 2008, "A High Efficiency Dual-Mode Buck Converter IC for Portable Applications," IEEE Trans. Power Electron., **23**(2), pp. 667–677.
[43] Liang, C., Dong, Z., Zhang, Q., Cao, T., Gao, X., Wang, N., and Zhang, Z., 2023, "Event-Triggered MPC for Current-Source-Mode Single-Inductor Multiple-Port DC-DC Converter," IEEE 14th International Symposium on Power Electronics for Distributed Generation Systems (PEDG), Shanghai, China, June 9–12, pp. 932–937.
[44] Fan, H., Li, Z., Wang, B., and Han, Y., 2023, "Influence of Parameter Mismatch on Event-Triggered MPC and Solution for Power Converters," IECON 2023-49th Annual Conference of the IEEE Industrial Electronics Society, Singapore, Oct. 16–19, pp. 1–5.
[45] Yang, Z., Li, S., Cao, K., Chen, D., Li, J., and Cao, W., 2025, "Event-Triggered Model Predictive Control of Buck Converter With Disturbances: Design and Experimentation," J. Low Power Electron. Appl., **15**(3), p. 45.
[46] Sun, J., 2012, "Pulse-Width Modulation," *Dynamics and Control of Switched Electronic Systems: Advanced Perspectives for Modeling, Simulation and Control of Power Converters*, Springer, London, UK, pp. 25–61.
[47] Geyer, T., Papafotiou, G., Frasca, R., and Morari, M., 2008, "Constrained Optimal Control of the Step-Down DC–DC Converter," IEEE Trans. Power Electron., **23**(5), pp. 2454–2464.
[48] Rawlings, J., Meadows, E., and Muske, K., 1994, "Nonlinear Model Predictive Control: A Tutorial and Survey," IFAC Proc. Vol., **27**(2), pp. 185–197.
[49] Karamanakos, P., Geyer, T., Oikonomou, N., Kieferndorf, F. D., and Manias, S., 2014, "Direct Model Predictive Control: A Review of Strategies That Achieve Long Prediction Intervals for Power Electronics," IEEE Ind. Electron. Mag., **8**(1), pp. 32–43.
[50] Karamanakos, P., and Geyer, T., 2020, "Guidelines for the Design of Finite Control Set Model Predictive Controllers," IEEE Trans. Power Electron., **35**(7), pp. 7434–7450.
[51] Chen, J., and Yi, Z., 2021, "Comparison of Event-Triggered Model Predictive Control for Autonomous Vehicle Path Tracking," IEEE Conference Control Technology and Applications (CCTA), San Diego, CA, Aug. 9–11, pp. 808–813.
[52] Li, H., and Shi, Y., 2014, "Event-Triggered Robust Model Predictive Control of Continuous-Time Nonlinear Systems," Automatica, **50**(5), pp. 1507–1513.
[53] Heemels, W. P., Johansson, K. H., and Tabuada, P., 2012, "An Introduction to Event-Triggered and Self-Triggered Control," 51st IEEE Conference on Decision and Control (CDC), Maui, HI, Dec. 10–13, pp. 3270–3285.
[54] Simon, D., 2006, *Optimal State Estimation: Kalman, H Infinity, and Nonlinear Approaches*, Wiley, Hoboken, NJ.